Branching instabilities in rapid fracture: Dynamics and geometry

Eran Bouchbinder, Joachim Mathiesen, and Itamar Procaccia

Deptartment of Chemical Physics, The Weizmann Institute of Science, Rehovot 76100, Israel

We propose a theoretical model for branching instabilities in 2-dimensional fracture, offering predictions for when crack branching occurs, how multiple cracks develop, and what is the geometry of multiple branches. The model is based on equations of motion for crack tips which depend only on the time dependent stress intensity factors. The latter are obtained by invoking an approximate relation between static and dynamic stress intensity factors, together with an essentially exact calculation of the static ones. The results of this model are in qualitative agreement with a number of experiments in the literature.

PACS number(s): 62.20.Mk, 46.50.+a, 81.40.Np, 83.60.Uv

I. INTRODUCTION

The phenomenon of crack division, i.e., the splitting of a single primary crack into two or more branches, whose dynamics develops independently, is studied in thin plates of different materials (glasses, plastics, metals etc.) [1]. A classical example from more than thirty five years ago is shown in Fig. 1, which exhibits a crack pattern observed in a thin araldite plate [2]. In this example the cracks go throughout the thickness of the sheet. This is to be distinguished from apparently similar side branching instabilities in which side branches appear in addition to the main crack, when the velocity of propagation exceeds a critical value [3,4]. There exists an important difference between the two phenomena: in the former cases all the branches crack through the plates (sometime referred to as "macrobranching"), whereas in the latter experiments, near the onset of the instability, the side branches have a width which is considerably smaller than the thickness of the plate (sometime referred to as "microbranching"). Notwithstanding attempts to interpret the latter phenomenon using 2-dimensional theories [5,6], it appears that the interaction of crack fronts of different thickness necessitates a 3-dimensional theory which is daunting at present. In this paper we limit our discussion to a 2-dimensional theory that pertains only to plates with cracks going through the plate.

The aim of this paper is to develop an approximate theory of crack dynamics, including crack bifurcations and multiple crack competition. More specifically, we address the following questions.

(1) Given a straight propagating crack in a 2-dimensional material, when and how the first bifurcation occurs? The bifurcation event itself was studied successfully in a recent paper by Adda-Bedia [5]. In our approach we are able to examine the dynamics of the bifurcated cracks.

(2) Given a bifurcated crack, what is the stability of a symmetric branched configuration? We show that there exists an instability towards geometric perturbations, making one branch growing on the expense of the other which gets arrested.

(3) What is the geometry of multiple (two or more) branches? Obviously the interaction between multiple branches results in curved cracks. The model that we propose

is able to follow the dynamics and the resulting geometry.

(4) How consecutive bifurcations come about, and what are the resulting crack patterns?

(5) Can one apply the 2-dimensional theory developed here to microbranching? The answer will be shown to be negative; there are crucial 3-dimensional aspects of microbranching that need the 3-dimensional theory in its entirety for an appropriate treatment.

In order to answer all these questions, we take the point of view that the dynamics of the tip of each crack is determined by the elastic field in its very vicinity. Near each tip one expands the stress field as usual,

$$\sigma_{ij}(r, \theta, t) = K_{\mathrm{I}}(t) \frac{\Sigma_{ij}^{\mathrm{I}}(\theta, v)}{\sqrt{2\pi r}} + K_{\mathrm{II}}(t) \frac{\Sigma_{ij}^{\mathrm{II}}(\theta, v)}{\sqrt{2\pi r}}. \tag{1}$$

Here v is the instantaneous tip velocity, $\{r, \theta\}$ are polar coordinates at the crack tip and t is time. $K_{\mathrm{I}}(t)$ and $K_{\mathrm{II}}(t)$ are the *dynamic* stress intensity factors, and the functions Σ are known universal functions of θ and v.

The central element in our model is the adoption of the Hodgdon-Sethna equations for the crack tips [7]. These equations were derived in the context of quasistatic crack propagation, and were shown to be in agreement with quasistatic experiments in [8]. Here we employ these equations in the dynamic context, invoking the results and their comparison with experiments for justification. Consider a local coordinates system located at the crack tip, in which $\hat{\mathbf{t}}$ and $\hat{\mathbf{n}}$ denote the tangential and normal directions respectively. For the crack tip location $\mathbf{r}^{tip}$ we write the equations
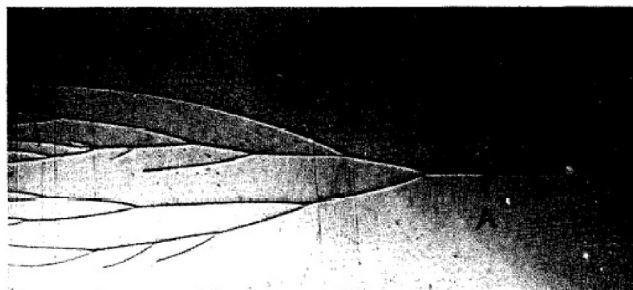

FIG. 1. Crack pattern in an araldite tensile sheet [2].

056118-1

$$\frac{\partial \mathbf{r}^{tip}}{\partial t} = v\hat{\mathbf{t}},$$

$$\frac{\partial \hat{\mathbf{t}}}{\partial t} = -fK_{\text{II}}(t)\hat{\mathbf{n}}. \tag{2}$$

Here v is the instantaneous crack tip velocity, and f is a positive material function. Note that the first of Eqs. (2) is nothing but a geometric kinematic relation that assumes local smoothness of the crack trajectory. The second equation results from symmetry considerations, but much physics is hidden in the material function f. Needless to say, these equations appear simpler than they really are. The actual calculation of the dynamic stress intensity factors for evolving cracks of complicated geometry is very far from trivial. The bulk of Sec. II is devoted to the presentation of approximate schemes to compute these objects. The main idea is to relate the dynamic stress intensity factors to their static counterpart [9], and then to compute the latter using the method of iterated conformal maps that had been presented for fracture problems in recent papers [10,11]. This material is reviewed in Sec. III.

Having at hand the stress intensity factors one can use them in Eqs. (2) for each crack tip. In Sec. IV we describe how this is done for multiple branch dynamics. We demonstrate that the theory is successful in describing crack bifurcations, crack arrest, and successive bifurcations. The geometry can be studied in great detail and compared with available experiments. Finally, in Sec. V we consider the applicability of this theory to microbranching. As mentioned above, the conclusion is negative. Section VI offers a summary of the paper and some concluding remarks.

II. DYNAMICS OF MULTIPLE CRACKS

To implement Eqs. (2) we need first to compute the dynamic stress intensity factors, and second the velocity v at the tip of each branch in a multiple branch configuration. We start with the stress intensity factors.

A. Estimating the dynamic stress intensity factors

The first task is the calculation of the *dynamic* stress intensity factors for a branched configuration. To this aim we invoke the formalism developed in [9], in which the dynamic stress intensity factors were related to their static counterparts. Based on some specific examples an approximate form of the *dynamic* stress intensity factors was obtained as a product of the *static* stress intensity factors K_{I}^{s} and K_{II}^{s} (of the instantaneous frozen configuration) and universal functions of the instantaneous velocity. For each mode of fracture one writes

$$K_{\text{I}}(t) \simeq k_{\text{I}}(v)K_{\text{I}}^{s}(t),$$

$$K_{\text{II}}(t) \simeq k_{\text{II}}(v)K_{\text{II}}^{s}(t). \tag{3}$$

We note that both the dynamic and the static stress intensity factors are considered time-dependent. For the static objects

this dependence means freezing the actual configuration that is obtained at time t. The universal functions of the velocity are given by

$$k_{\text{I}}(v) = S\left(-\frac{1}{v}\right)\frac{1 - v/c_R}{\sqrt{1 - v/c_d}},$$

$$k_{\text{II}}(v) = S\left(-\frac{1}{v}\right)\frac{1 - v/c_R}{\sqrt{1 - v/c_s}} \tag{4}$$

and $S(\zeta)$ is given by

$$S(\zeta) = \exp\left[-\frac{1}{\pi}\int_{1/c_d}^{1/c_s} \tan^{-1}\left(\frac{4\eta^2\sqrt{(\eta^2 - c_d^{-2})(c_s^{-2} - \eta^2)}}{(c_s^{-2} - 2\eta^2)^2}\right)\right.$$

$$\left.\times\frac{d\eta}{\zeta + \eta}\right]. \tag{5}$$

Here c_R, c_d and c_s are the Rayleigh, dilatational and shear wave speeds, respectively.

This approximation was shown in the classical theory of fracture mechanics to be essentially exact for semi-infinite straight cracks [12]. In our earlier work we applied this approximate methodology for describing interacting large and small cracks [9]. The separable form of the dynamic stress intensity factors is trivially correct for very small velocities, since the functions k_{I} and k_{II} tend to unity for $v\to 0$. For finite velocities the separable form is not exact, but we expect it to yield good approximations when the velocities are small fractions of the typical wave speed and the typical distance between the evolving tips is small. In fact, when there are more wave reflections between the various branches of our crack, the better is the approximate form. Once two or three wave reflections have taken place the dominant dynamic interaction is the self interaction of the crack tip with its immediate vicinity, and the dynamical part of this interaction is fully contained in the functions k_{I} and k_{II}. Physically stated, under the specified conditions the waves deliver the required mechanical information that makes the approximation tenable. We will demonstrate below that such conditions are satisfied throughout the dynamics of the branching instability, therefore allowing us to use the separable form quite confidently in the present context. Nevertheless it should be stated that it is difficult to quantify *a priori* the range of validity of the approximation. Therefore we invoke the final results and their agreement with various experimental results to support the quality of the approximation.

Clearly, this approximation is a huge simplification, calling for solving the static equilibrium field equations rather than the full dynamical field equations. Of course, one still has to face the difficult problem of *static* non-trivial geometries, but this problem was solved quite *generally* using the method of iterated conformal maps [10], and demonstrated in the context of complex crack geometries in [11].

B. The velocity of the crack tips

To close Eqs. (2) as a consistent mathematical system we need to compute the velocity of each tip in terms of the

dynamic stress intensity factors. The basic idea is to employ the energy balance that equates the energy release rate into the crack tip region (denoted by G) to the dissipation involved in the crack propagation (denoted by Γ). The classical theory of linear elasticity fracture mechanics [12] provides the energy release rate into each tip region:

$$G = \frac{1-\nu^2}{E}[A_{\mathrm{I}}(v)K_{\mathrm{I}}^2 + A_{\mathrm{II}}(v)K_{\mathrm{II}}^2], \qquad (6)$$

where E and ν are the Young's modulus and Poisson's ratio, respectively, and $A_{\mathrm{I}}(v)$ and $A_{\mathrm{II}}(v)$ are universal functions given by

$$A_{\mathrm{I}}(v) = \frac{v^2\sqrt{1 - v^2/c_d^2}}{(1-\nu)c_s^2 D(v)},$$

$$A_{\mathrm{II}}(v) = \frac{v^2\sqrt{1 - v^2/c_s^2}}{(1-\nu)c_s^2 D(v)},$$

$$D(v) = 4\sqrt{(1 - v^2/c_d^2)(1 - v^2/c_s^2)} - (2 - v^2/c_s^2)^2. \qquad (7)$$

Note that $D(v)$ vanishes at the Rayleigh wave speed, $v = \pm c_R$.

For concreteness, consider a two-dimensional infinite medium loaded at infinity with a uniform constant tensile stress σ_{yy}^∞. A long straight crack propagates at an instantaneous velocity V; at some critical velocity, when the crack length is L, the crack bifurcates into two branches of lengths $\{\ell_i\} \ll L$ with tip velocities $\{v_i\}$, defining angles $\{\lambda_i\pi\}$ with respect to the direction of the crack prior to the bifurcation. Freezing the crack just at the bifurcation we denote its static stress intensity factor as $K_{\mathrm{I}}^{(0)}$.

At each tip of the bifurcated crack we define the normalized stress intensity factors

$$F_{\mathrm{I}} = \frac{K_{\mathrm{I}}^s}{K_{\mathrm{I}}^{(0)}}, \qquad F_{\mathrm{II}} = \frac{K_{\mathrm{II}}^s}{K_{\mathrm{I}}^{(0)}}. \qquad (8)$$

Equating G to Γ we can rewrite Eq. (6) at *each branch tip* as

$$\frac{E\Gamma}{1-\nu^2} = g_{\mathrm{I}}(v)F_{\mathrm{I}}^2[K_{\mathrm{I}}^{(0)}]^2 + g_{\mathrm{II}}(v)F_{\mathrm{II}}^2[K_{\mathrm{I}}^{(0)}]^2, \qquad (9)$$

with

$$g_{\mathrm{I}}(v) \equiv A_{\mathrm{I}}(v)k_{\mathrm{I}}^2(v),$$

$$g_{\mathrm{II}}(v) \equiv A_{\mathrm{II}}(v)k_{\mathrm{II}}^2(v). \qquad (10)$$

Under the assumption that Γ is velocity independent we observe that the left-hand side of Eq. (9) contains only material parameters. Therefore, a similar equation holds for the pure mode I crack propagating with velocity V_b just before the branching event,

$$\frac{E\Gamma}{1-\nu^2} = g_{\mathrm{I}}(V_b)[K_{\mathrm{I}}^{(0)}]^2. \qquad (11)$$

We conclude that the instantaneous velocity v_i of each crack tip is determined by V_b according to

$$g_{\mathrm{I}}(V_b) = g_{\mathrm{I}}(v_i)F_{\mathrm{I}}^2 + g_{\mathrm{II}}(v_i)F_{\mathrm{II}}^2 \quad \forall \ i. \qquad (12)$$

Note that it would be better to index the stress intensity factor with an index i to stress that each tip contributes its own equation to the set. We avoid it in order not to overburden the notation. Notwithstanding, in case for which the dissipation function Γ becomes velocity dependent, we should introduce $\Gamma(v_i)/\Gamma(V_b)$ on the left-hand side (LHS) of Eq. (12). Bearing in mind that $g_{\mathrm{I}}(V_b)$ is a decreasing function, the result of such a change would be a reduction in V_b [5].

On physical grounds one seeks solution of these relations for non-negative branch velocities v_i. In Ref. [5] it was shown that under the *assumption* that the branches start their evolution quasi-statically (i.e., $v_i=0$) a solution appears first for symmetric branching at $V_b=v_c \approx 0.475c_s$. For higher velocities $V_b > v_c$ one can have bifurcations in which the branches start off at a finite velocity.

Finally, we bring the equations of motion to their final form as used below. We have no experimental information about the material function f in Eqs. (2). Accordingly we will assume f constant, measure velocities in units of c_s, and length in units of $c_s/fK_{\mathrm{I}}^{(0)}$. Let θ be the angle between the tangential unit vector and the x axis. Denoting the tip position of the straight crack at bifurcation as $\mathbf{r}_b$, $\ell_i \equiv |\mathbf{r}_i^{tip} - \mathbf{r}_b|$. We rewrite now the tangential and normal unit vectors at the tip of the crack in terms θ and a rescaled time $tK_{\mathrm{I}}^{(0)}f \to t$. These changes transform Eqs. (2) into

$$\frac{\partial \ell_i}{\partial t} = v_i,$$

$$\frac{\partial \theta_i}{\partial t} = -k_{\mathrm{II}}(v_i)F_{\mathrm{II}}. \qquad (13)$$

These equations, in conjunction with Eqs. (12), define our dynamical system. Note that the velocities are measured in units of c_s. We selected $\nu=0.25$ which implies $c_d=\sqrt{3}c_s$ and $c_R=0.9194c_s$. It is important to notice that the set of equations for each branch tip is coupled to the equations for the other tips via the functions F_{I} and F_{II}. All the results presented below are obtained by the following procedure: for each instantaneous branched configuration the functions F_{I} and F_{II} are calculated using the method of iterated conformal mappings, then the velocities of the tips are calculated using Eqs. (12) and finally the increments in length and angle are calculated according to Eqs. (13).

III. STATIC BRANCHED CONFIGURATIONS

A crucial ingredient in our model is the calculation of the *static* stress intensity factors for an arbitrary branched crack configuration. The general approach to this problem, based on the method of iterated conformal mappings, is presented in all detail in Ref. [10]. The essential building block is the composition of the conformal map from the exterior of the unit circle to the exterior of the complicated crack shape, using a functional iteration of a fundamental conformal map that adds one single bump to the unit circle. This scheme enables us to solve for the entire stress field for any branched
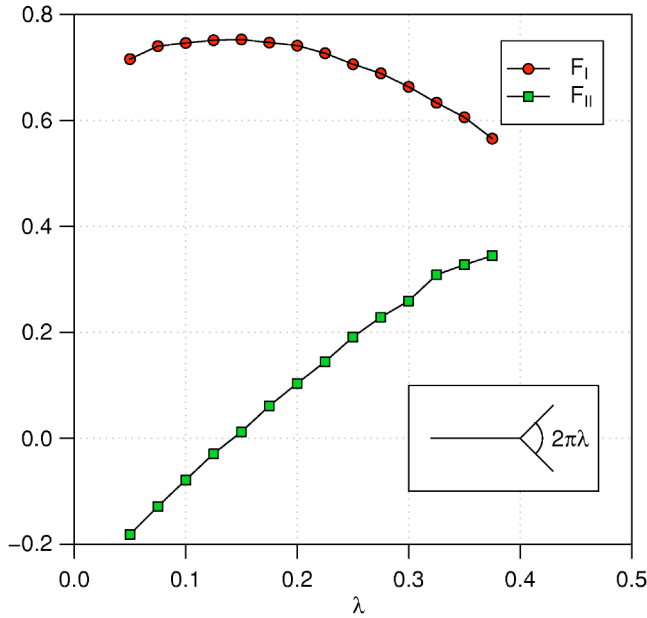
FIG. 2. The normalized stress intensity factors F_I and F_{II} as a function of λ, where $2\pi\lambda$ is the angle between the branches (see inset). The ratio of branch length and the main crack is $\ell/L=0.5 \times 10^{-3}$.

FIG. 3. The normalized stress intensity factors F_I and F_{II} for both tips as a function of λ, where $\pi\lambda$ is the angle between the branches (see inset). The ratio of branches length and the main crack is $\ell/L=0.5\times10^{-3}$.

crack configuration. The static stress intensity factors are extracted from the near tip fields using the method explained in [10]. In the present context the crack tips are dressed by a finite curvature determined by the size of the bump of the fundamental map which is added at each iteration. While appropriate for comparison with most realistic experiments, where some blunting of the crack tip is always present, this finite curvature means that comparison with mathematical models with infinitely sharp cracks should be done with care.

In the literature there is only limited amount of works presenting calculations of stress intensity factors for in-plane problems with branched crack configurations. In Ref. [5] such a calculation for an infinitesimal symmetric branched configuration is provided using a numerical solution of an integral equation. In order to ascertain the reliability and accuracy of our calculation we consider first a similar configuration, choosing the length ℓ of each branch such that $\ell/L =0.5\times10^{-3}$. We could not select a smaller ratio due to the finite curvature of the crack tip (in addition, our numerical scheme which is based on truncated Fourier expansions cannot deal efficiently with minute geometric details, since the series truncation becomes inaccurate). The normalized stress intensity factors F_I and F_{II} as a function of λ, where $2\pi\lambda$ is the angle between the branches (see inset) are shown in Fig. 2. This figure should be compared with Fig. 4 in Ref. [5]. It is clear that the figures are in good agreement (the locations of the maximum of F_I and zero crossing of F_{II} are nearly identical), although there is a slight overestimation in F_I due to finite size effects.

Second, we considered an asymmetric branched configuration in which both branches have the same length $\ell/L =0.5\times10^{-3}$, while one of them is located in the direction of the main crack and the other creates an angle of $\pi\lambda$ relative to that direction. The normalized stress intensity factors F_I
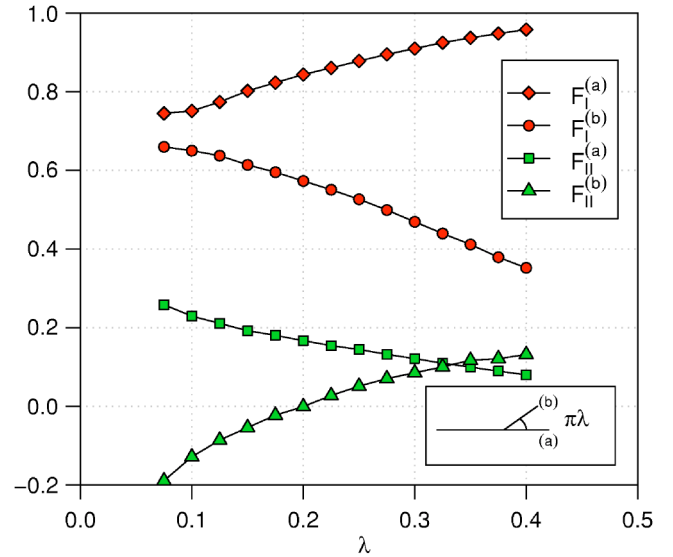
and F_{II} for both tips as a function of λ are shown in Fig. 3. To our best knowledge there is no calculation available in the literature for this configuration. Since mode III models are usually in a qualitative agreement with their in-plane counterparts we present in the Appendix the calculation for a mode III asymmetric branched configuration and present the resulting normalized stress intensity factors in Fig. 4. Indeed, the mode I component of the in-plane calculation shows the same qualitative behavior as its mode III counterpart.
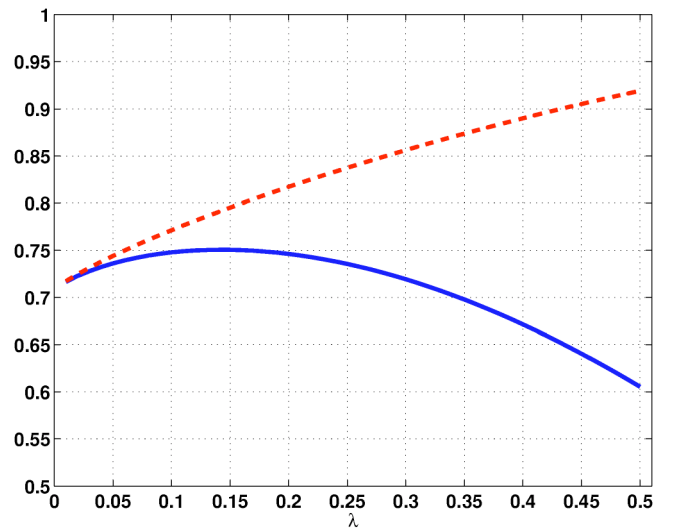

FIG. 4. The mode III normalized stress intensity factor for an asymmetric branched configuration. $\pi\lambda$ is the angle between the branches and the ratio of the branches length and the main crack length is $\ell/L=0.5\times10^{-3}$. The upper (lower) curve corresponds to the forward direction (inclined) branch.

IV. THE DYNAMICS OF MULTIPLE BRANCHES

In Ref. [5] it was found that under the conditions that the branches start off quasistatically (with zero velocity) and with $K_{II} \approx 0$, the critical velocity is $V_b = v_c \approx 0.475 c_s$ and the branching angle $\lambda \pi$ is 0.13π. Note that λ is determined by the zero crossing of K_{II} presented in Fig. 2. The velocity is "critical" in the sense that it is the first velocity for which branching is energetically possible. Since there is no specification of the mechanism of branching, one should treat it as a lower bound for the branching velocity. For every $V_b > v_c$ one can find a solution with the same λ (since it is determined by the independent condition $K_{II} \approx 0$), but with a nonvanishing velocity of the branches. Indeed, experimentally it appears that the branches do not emerge quasistatically as implied by the solution of [5]. Note that as long as V_b is not much larger than v_c, the branches velocities are relatively small. Bearing in mind that the distance between the tips is also relatively small, we can use the separable form of the dynamic stress intensity factors quite confidently. In this section we analyze the post-branching dynamics for various physical conditions.

A. Stability analysis

Motivated by the experimental evidence that symmetric branches do not emerge quasistatically [13,14], we study the stability of the symmetric configuration against small geometrical perturbations. We consider the possibility that dynamical instabilities prevent the development of the branching event even though it is energetically allowed at $V_b = v_c$. Consider a symmetric branched configuration with $\ell/L = 0.5 \times 10^{-3}$ and $\lambda = 0.13$. Introduce a positive small perturbation $\delta\ell = 0.5 \times 10^{-2}\ell$ to the length of one of the branches, and integrate the dynamical Eqs. (12) and (13) for various $V_b > v_c$. Note that as V_b increases so does the velocity of the emerging branches. Figure 5 presents the resulting dynamics for $V_b = 0.50$ and $V_b = 0.55$. A representative resulting crack pattern is shown in the inset; the unperturbed branch competes with the perturbed one and eventually dies out (i.e., it gets arrested due to screening effects). The velocities of the branches are plotted as a function of time. The time to arrest can be identified as the point where the velocity of the unperturbed branch vanishes. By comparing the data for the two branching velocities, it is clear that the time to arrest increases substantially as V_b increases, therefore we deduce that the increment of instability *decreases* with increasing V_b. We conclude that symmetric branched configurations are unstable against small geometrical perturbations at least for the branching velocities we considered. We should stress that larger V_b's are not considered here due to the expected deterioration in the quality of the approximation embodied in the separable form of the dynamic stress intensity factors. In this regime it is reasonable to believe that other dynamic effects are important and might stabilize the symmetric configuration. In particular if the function $\Gamma(v)$ is an increasing function of the velocity, then the faster and longer branch would be relatively punished and its velocity would reduce, allowing the shorter branch to catch up. Similarly a velocity dependence of $f(v)$ may contribute further stabilizing factors.
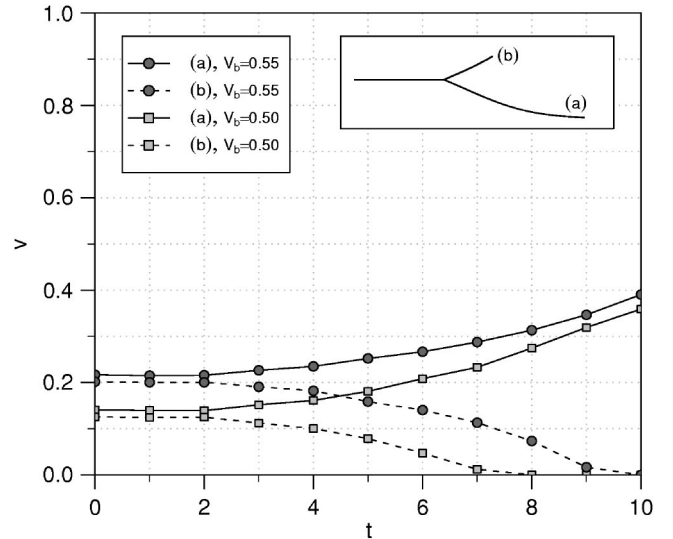

FIG. 5. The velocities of the branches as a function of time for $V_b = 0.50$ and $V_b = 0.55$. The resulting dynamics are such that the unperturbed branch is arrested, while the perturbed one returns after a short time to the original crack path. A representative resulting crack pattern is shown in the inset. See text for details.

The resulting dynamics are such that the unperturbed branch is arrested, while the perturbed one returns after a short time to the original crack path. Therefore, the main effect of these attempted branching events is the sudden deceleration of the crack. We suggest to interpret the instability as a possible explanation for the fact that in macrobranching events the branches do not emerge quasistatically [13,14] since then the configuration is very sensitive to perturbations and probably cannot be observed on macroscopic scales. On the other hand, for larger branching velocities, for which the branches emerge with finite velocities, both branches coexist, they are less unstable to small perturbations and therefore can grow to observable sizes.

In the framework of stability analysis we also consider the final length of the arrested branch. Denoting by $\Delta\ell$ the difference between the final branch length and its initial length ℓ, we show in Fig. 6 the relative change in length $\Delta\ell/\ell$ as a function of V_b for two values of the fixed ratio $\delta\ell/\ell$. The dependence seems to be approximately linear for both. Note that the continuation of the lines intersects the x axis at the critical branching velocity $V_b = v_c \approx 0.475$, below which branching is energetically forbidden. In passing, we note the resemblance of Fig. 6 to the experimental results obtained in [3] for the microbranching instability. There it was found (see Fig. 3 in [3]) that the branch length increases approximately linearly with the mean crack velocity and vanishes for the critical one.

B. Successive branching events

In light of the observation of asymmetric branch growth with one of them arrested, we follow now the evolution of the surviving branch. This branch then accelerates to the critical branching velocity and may bifurcate again. In this subsection we study the patterns formed by such multiple
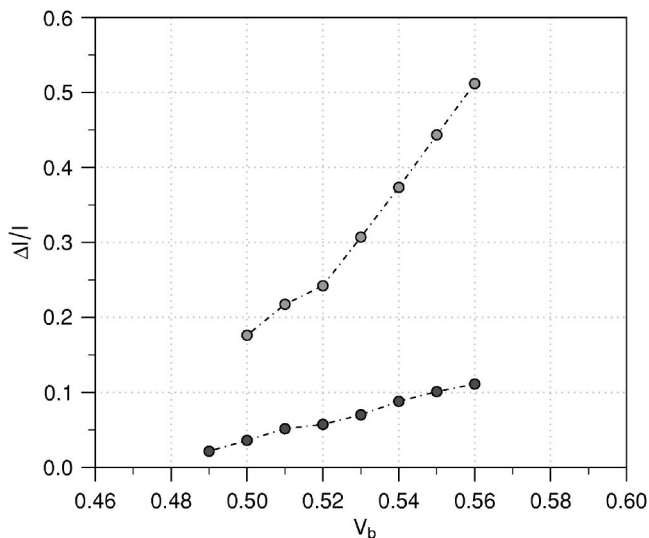
FIG. 6. The relative change in length $\Delta\ell/\ell$ as a function of V_b for $\delta\ell=2\times10^{-2}\ell$ (lower curve) and $\delta\ell=0.5\times10^{-2}\ell$ (upper curve). Note that the continuation of the lines intersects the x axis at the critical branching velocity $V_b=v_c\approx0.475$, below which branching is energetically forbidden.

FIG. 8. A crack pattern in a tensile $260\times120\times5$ mm araldite plate [1]. The plate was notched symmetrically at the edge. Due to minute asymmetries in the production of the notches, only one of them propagates. A second branching event can be observed after some time. In this event almost symmetric branches emerge from the branching point and coexist until one outruns the other and then curves towards the symmetry line. Attempted branching events can be clearly observed before the successful branching event took place. All these features are in qualitative correspondence with our discussion.

successive branching events. In Fig. 7 we present the crack pattern that was formed by three successive branching events. At the first event we introduced a positive small perturbation $\delta\ell=2\times10^{-2}\ell$ to the length of the lower branch. At the second event we introduced a symmetric configuration with the same ℓ and λ with no perturbation added by hand. We stopped the evolution of the system at the onset of the third event since within our numerical precision we could not determine its outcome; in some cases it turned out that the upper branch outruns the lower and in others vice versa. The results shown in Fig. 7 are in qualitative agreement with the experimental results shown in Fig. 8. Unfortunately we cannot offer a quantitative comparison due to the paucity of experimental details, in particular the time dependence of the crack evolution. In our theory velocities and lengths are rescaled as explained above, and we therefore can compare only the postmortem geometry.

We note here that the seemingly up-down anti-correlation between the winning branches of successive events in Fig. 7 is reminiscent of the spatial ordering observed in the micro-

branching instability (see Fig. 4c in [4]). This similarity, in conjunction with the resemblance discussed in relation with Fig. 6, suggests that our 2-dimensional theory might have captured some of the features of the microbranching instability, although it cannot be directly applied in that case (see Sec. V).

C. Symmetric branching

As discussed above, at higher branching velocities, symmetric branches can coexist for a longer time, and it is interesting to determine the typical profiles of such symmetric branches. Consider an experiment in which a crack of length L in a long strip of width W bifurcates and two symmetric branches of length ℓ emerge. As the branches start propagating with $K_{II}\approx0$, they cannot change their direction as long as $\ell\ll L,W$. On the other hand, when ℓ grows to the order of the smaller between L and W, the branches will curve. In our theory there is only one length L (the system is infinite) and we study the curving of branches of length comparable to L.

Figure 9 shows several branching scenarios for different branching length L. It is tempting, after the example of [3], to fit power laws to these profiles. The different profiles can be approximated in the limited range that we consider by a power law $y\sim x^{\zeta}$ with $0.7<\zeta<0.8$. The fit in the figure corresponds to $\zeta=0.8$ and was added as a guide for the eye. It should be immediately said however that the profiles are neither universal nor true power laws. They represent a transient behavior between two straight lines. Initially the branches start off with an angle $\lambda\pi=0.13\pi$. Finally there is an asymptotic fixed angle that depends on the geometry of the system. In an infinite medium this final angle satisfies $0<\lambda<0.13$, while in a strip of finite width $\lambda=0$, i.e., the branches propagate eventually parallel to the boundaries of the strip.
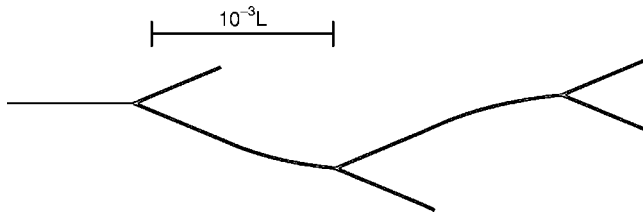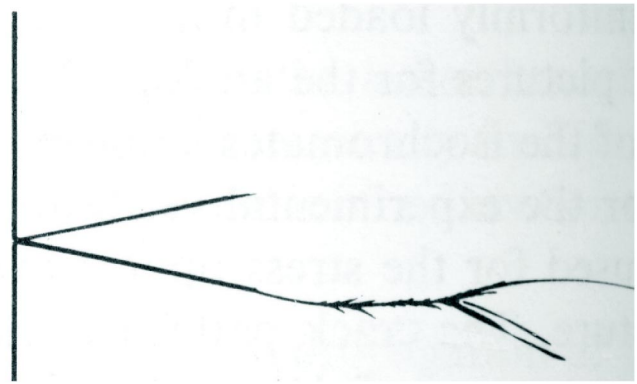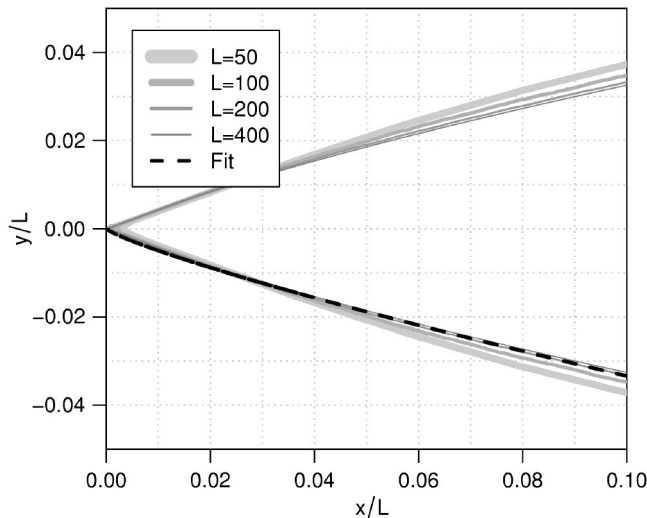

FIG. 7. The crack pattern that was formed by three successive branching events. The branching velocity was set to $V_b=0.5$, i.e., slightly more than v_c. We introduced a positive small perturbation $\delta\ell=2\times10^{-2}\ell$ to the length of the lower branch. Upon reaching the branching velocity again we introduced a symmetric configuration with the same ℓ and λ with no perturbation added by hand. The bar shows the scale of the process relative to the initial crack length L.

FIG. 9. Symmetric branching dynamics for different branching length L with $V_b=0.5$. The plot shows the various crack patterns in rescaled coordinates. A power law $y \sim x^\zeta$ with $\zeta=0.8$ was added as a guide for the eye.

As an example of the relevance of our calculation to actual crack branching events, Fig. 10 shows two shadow photographs of different stages of a symmetric branching event in a glass plate [1]. The left panel shows the onset of branching with straight branches as long as ℓ is smaller than L and W. The right panel shows the developed branching configuration. The similarity with Fig. 9 is obvious.

V. HOW ABOUT MICROBRANCHING?

With the relative success of the model proposed here in reproducing the typical geometry of macrobranches it is of course tempting to see whether also the geometry of microbranches can be gleaned from the present 2-dimensional theory. To this aim we have attempted to follow the dynamics of a side branch in an asymmetric configuration in which the main branch is forced to emerge in the forward direction, see the inset of Fig. 3. We selected $\lambda=0.2$ such that K_{II} of the side branch is approximately zero. This initial configuration was introduced as a constraint on the system to reflect the local symmetry breaking observed in experiments [3]. Generally, this asymmetry results in a velocity difference between the side branch and the main branch.
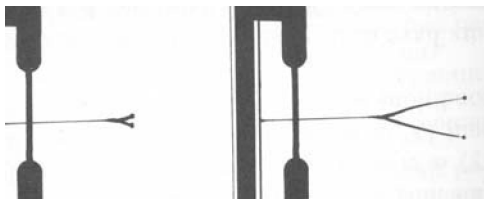

FIG. 10. Two shadow photographs of a symmetric branching event in a $300 \times 100 \times 9$ mm glass plate [1]. The left panel shows the early stages of the branching process where the branches are almost straight, while the right panel shows the developed curved branching configuration.
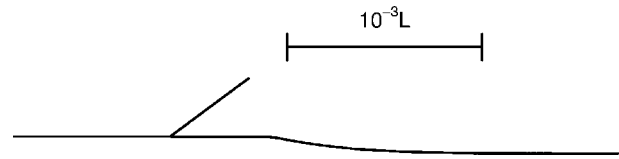

FIG. 11. A typical resulting configuration for asymmetric branching. The side branch is almost immediately arrested, while the main branch temporarily deflected from its straight path. The net effect of such an event is a strong fluctuation in the velocity of the main branch. The bar shows the scale of the process relative to the initial crack length L.

Figure 11 shows a typical resulting configuration in which the velocity of the main branch fluctuates in a way similar to the experimentally observed velocity fluctuations, while the side branch was almost immediately arrested. Since we were mainly interested in the dynamics of the side branch, i.e., its trajectory and lifetime, we concluded that a model that treats the main macroscopic branch and the microscopic side branch on equal footings is doomed to fail. The meaning of this result is that the energy flux into the microscopic side-branch is dramatically *underestimated* in a 2-dimensional model. We tried to increase artificially the energy release rate G into the near tip region of the side branch by a constant factor, such as to increase its initial velocity. Nevertheless, the velocity of the side branch dropped immediately to zero, reflecting the huge screening effect of the main branch. Therefore, although some of our results in Sec. IV show similarities with various features of the microbranching instability, we propose that the phenomenon of microbranching is essentially 3-dimensional and cannot be modeled directly by a 2-dimensional theory.

VI. SUMMARY AND CONCLUSIONS

In summary, we have introduced dynamical equations of motion for crack tips which depend only on the stress intensity factors at the tips. Generally speaking, the calculation of these objects is daunting. By adopting an approximate separable form for the dynamic stress intensity factors in terms of their static counterparts and universal velocity dependent functions we achieved a huge simplification that results in tractable dynamics. Instead of complicated field equations we can reduce the theory to ordinary differential equations for the crack tips. Complex events like crack bifurcations, branch competition, branch arrest and successive bifurcations are studied in detail and compared with experiments. The good news is that the comparison with experiments is encouraging; more quantitative comparisons call for new experiments that will take into account the proposed insights, including measuring $f(v)$. The bad news is that the quality of the approximation cannot be easily assessed from first principles. One expects that for low velocities and small distances between the multiple crack tips the approximation should be quite good. What is the range of validity can at this point be gleaned only from comparison with experiments, and these are relatively old and not detailed enough, maybe giving the false impression of a good agreement. It thus

seems very worthwhile to conduct *new* experiments in light of this theory in order to test it in some detail. The gained transparency and simplicity of the theory seems a very good motivation for such an undertaking.

ACKNOWLEDGMENTS

APPENDIX: STATIC MODE III ASYMMETRIC BRANCHING

The aim of this appendix is to derive the static stress intensity factors at the tips of an asymmetric branched mode III configuration. Since the mode III problem is described by Laplace equation for the displacement field $u_z(x,y)$

$$\nabla^2 u_z(x,y) = 0, \tag{A1}$$

the solution of this problem is readily given if the conformal map, $z = \Phi(\omega)$, from the exterior of the unit circle to the exterior of a branched crack configuration is known. The general formalism for obtaining such a map is known in the literature for a long time [2]. Here we adapt the general formalism to the problem at hand and solve it. Consider the following map

$$\Phi(\omega) = A\omega^{-1}(w - e^{i\alpha_1})^{\lambda_1}(w - e^{i\alpha_2})^{\lambda_2}(w - e^{i\alpha_3})^{\lambda_3}, \tag{A2}$$

where A is a real constant, $0 < \alpha_1 < \alpha_2 < \alpha_3 < 2\pi$ and $\lambda_3 = 2 - \lambda_1 - \lambda_2$. The points $\{e^{i\alpha_k}\}$ are mapped to the origin and therefore are branch points. For $\alpha_{k-1} < \theta < \alpha_k$ the phase of $\Phi(\omega)$ is fixed by the crack branch angle and a local maximum of $|\Phi(\omega)|$ is obtained at $e^{i\beta_k}$. The parameters of the map, i.e., A, $\{\alpha_k\}$ and $\{\beta_k\}$, can be calculated by demanding that for $\omega = 1$ $\arg(z) = 0$ and by the conditions $\Phi'(e^{i\beta_k}) = 0, |\Phi(e^{i\beta_k})| = \ell_k$. Here $\{\ell_k\}$ are the lengths of the crack branches. These three conditions can be translated into the following set of equations

$$\sum_{j=1}^{3} \alpha_j \lambda_j = 2\pi,$$

$$\sum_{j=1}^{3} \lambda_j \cot\left(\frac{\alpha_j - \beta_k}{2}\right) = 0,$$

$$4A\prod_{j=1}^{3}\left|\sin\left(\frac{\beta_k - \alpha_j}{2}\right)\right|^{\lambda_j} = \ell_k, \tag{A3}$$

which can be solved numerically. Having the conformal map for the required configuration at hand we are mainly inter-

ested in the stress intensity factors for the various crack tips. The solution for Eq. (A1) is given by

$$u_z(x,y) = \frac{1}{2\mu}[\varphi(z) + \overline{\varphi(z)}], \tag{A4}$$

where $\varphi(z)$ is an analytic function. The stress components in polar coordinates are given by

$$\sigma_{rz}(r,\theta) - i\sigma_{\theta z}(r,\theta) = e^{i\theta}\varphi'(re^{i\theta}) = e^{i\theta}\frac{\widetilde{\varphi}'(\omega)}{\Phi'(\omega)}. \tag{A5}$$

Here the tilde denotes the usual transplantation. In the near vicinity of a given crack tip z_k we use the following expansion:

$$\sigma_{rz}(r,\theta) = \frac{K_{\mathrm{III}}}{\sqrt{2\pi r}}\sin(\theta/2) + \mathcal{O}(\sqrt{r}),$$

$$\sigma_{\theta z}(r,\theta) = \frac{K_{\mathrm{III}}}{\sqrt{2\pi r}}\cos(\theta/2) + \mathcal{O}(\sqrt{r}). \tag{A6}$$

These two equations can be rewritten as

$$\sigma_{rz}(r,\theta) - i\sigma_{\theta z}(r,\theta) = \frac{-ie^{i\theta/2}K_{\mathrm{III}}}{\sqrt{2\pi r}} + \mathcal{O}(\sqrt{r}). \tag{A7}$$

On the other hand, near the crack tips we can expand the conformal map to obtain

$$z - z_k = \Phi(\omega) - \Phi(\omega_k) \simeq \frac{1}{2}\Phi''(\omega_k)(\omega - \omega_k)^2,$$

$$\Phi'(\omega) \simeq \Phi''(\omega_k)(\omega - \omega_k) = \sqrt{2\Phi''(\omega_k)(z - z_k)}. \tag{A8}$$

The last expression, in the light of Eq. (A5), shows the explicit relation between the square root singularity of the stress field near the crack tip and the derivative of the conformal map. Let us denote $z - z_k = re^{i(\delta_k\pi + \theta)}$ with $\delta_k = \sum_{j=1}^{k-1}\lambda_j$ and consider the direction tangent to the crack tip, i.e., $\theta = 0$. By comparing Eq. (A5) with Eq. (A7) we obtain

$$K_{\mathrm{III}} = i\widetilde{\varphi}'(\omega_k)\sqrt{\frac{\pi}{\Phi''(\omega_k)e^{i\delta_k\pi}}}. \tag{A9}$$

With this result at hand we can calculate the stress intensity factor at each tip since the solution in the ω plane is known to be

$$\widetilde{\varphi}(\omega) = -i\sigma_{yz}^{\infty}A[\omega - \omega^{-1}], \tag{A10}$$

where σ_{yz}^{∞} is the applied stress at infinity. Now we are in a position to analyze infinitesimal asymmetric branched configurations. We choose $\ell_1 = L$, $\ell_2 = \ell_3 = \ell$, $\lambda_1 = 1 - \lambda$ and $\lambda_2 = \lambda$ with $\ell/L = 0.5 \times 10^{-3}$. The resulting stress intensity factors are presented in Fig. 4 in the text.

[1] J. F. Kalthoff, *Dynamic Crack Propagation* (Noordhoof, Leyden, 1973), p. 449.

[2] H. Andersson, J. Mech. Phys. Solids **17**, 405 (1969).

[3] E. Sharon, S. P. Gross, and J. Fineberg, Phys. Rev. Lett. **74**, 5096 (1995).

[4] E. Sharon and J. Fineberg, Phys. Rev. B **54**, 7128 (1996).

[5] M. Adda-Bedia, J. Mech. Phys. Solids **53**, 227 (2005).

[6] M. Adda-Bedia, Phys. Rev. Lett. **93**, 185502 (2004).

[7] J. A. Hodgdon and J. P. Sethna, Phys. Rev. B **47**, 4831 (1993).

[8] E. Bouchbinder, G. Hentschel, and I. Procaccia, Phys. Rev. E **68**, 036601 (2003).

[9] E. Bouchbinder, D. Kessler, and I. Procaccia, Phys. Rev. E **70**, 046107 (2004).

[10] E. Bouchbinder, J. Mathiesen, and I. Procaccia, Phys. Rev. E **69**, 026127 (2004).

[11] E. Bouchbinder, J. Mathiesen, and I. Procaccia, Phys. Rev. Lett. **92**, 245505 (2004).

[12] L. B. Freund, *Dynamic Fracture Mechanics* (Cambridge University Press, Cambridge, England, 1998).

[13] H. Schardin in *Fracture*, edited by B. L. Averbach (MIT, Cambridge, MA, 1959), p. 297.

[14] K. Ravi-Chandar and W. G. Knauss, Int. J. Fract. **26**, 141 (1984).